An Impedance-Based Active Filter for Harmonic Damping by Type-IV Wind Turbines

Guest, Emerson; Rasmussen, Tonny Wederberg; Jensen, Kim H.

Published in:
Proceedings of 17th Wind Integration Workshop

Publication date:
2018

Document Version
Peer reviewed version

An Impedance-Based Active Filter for Harmonic Damping by Type-IV Wind Turbines

Emerson Guest and Tonny W. Rasmussen
Center for Electric Power and Energy
Technical University of Denmark, Lyngby DK-2800, Denmark
Email: edagu@elektro.dtu.dk

Kim H. Jensen
Siemens Gamesa Renewable Energy A/S
Brande DK-7330, Denmark

***Abstract*—In this paper, an impedance-based active filter is developed for the three-phase grid-connected converter used in a Type-IV wind turbine. The active filter utilizes the voltage and current measurement to provide programmable narrow-band shaping of the converter impedance. This has application in mitigating voltage or current amplification in wind power plants by increasing the harmonic damping applied by the wind turbines. Moreover, the active filter inherently compensates converter generated voltage harmonics, ensuring the voltage quality of the wind turbine. The performance of the active filter is verified through experiments on a 0.6MW grid-connected converter.**

I. Introduction

It is a common goal of both suppliers and consumers of power to reduce the harmonic distortion that they impose on other users of the power system. Harmonic producing loads draw non-sinusoidal currents through the power system resulting in harmonic voltage distortion at network buses [1]. Standards such as IEC-61000-3-6 [2] and IEEE-519:2014 [3] provide planning levels for consumers of power to ensure the harmonic currents drawn remain within acceptable limits. Suppliers of power are similarly advised by the standards but with the recommendation, instead, based on ensuring the quality of the voltage supply. This involves compensating for voltage harmonics and/or providing additional *harmonic damping* to the power system [4].

Power system resonances are known to cause voltage or current amplification at network buses [1],[5]-[8]. Offshore wind power plants (WPPs) are notorious for exhibiting such resonances between the shunt capacitance of the collector system, harmonic filters and capacitor banks, and the series inductance of power transformers. To make matters worse, the offshore platform is a significant contributer to the overall WPP cost and is thus highly optimized for space. Risk and uncertainty ensues for passive harmonic filter design and ensuring grid code compliance [9]. One proposed counter-measure has been to use a static compensator (STATCOM) at the onshore point of common coupling (PCC) of the WPP for active mitigation of voltage or current amplification at targeted frequencies [9],[10]. However, STATCOMs are not always available in a WPP and cannot eliminate harmonic sources generated by wind turbines. Accordingly, using the converters within the wind turbines of a WPP as an active filter has attracted the interest of wind turbine manufacturers, WPP developers and WPP owners [11].

Active filters used for harmonic damping do so by modifying the converter impedance within certain frequency ranges [4]. Such active filters have been termed *impedance-based* active filters [12] as programmed steady-state impedances/admittances tune the impedance shaping. The earliest active filters came from Akagi *et al.* [4] and achieved *wideband* damping by feeding-forward the measured voltage, scaled by a programmed conductance, to a hysteresis current controller. Converters employing linear current or voltage controllers have tended to use *narrow-band* active filters to reshape the converter impedance within a narrow frequency range. This has been achieved through feed-forward of the measured voltage [13] or current [14] after filtering by a sliding discrete Fourier transform (DFT). Alternatively, synchronous-frame lowpass filters cascaded with resonant filters have been used to achieve programmable harmonic impedance shaping [15].

In this paper, an impedance-based active filter based on a complex resonator and feed-forward of the measured voltage *and* current is proposed for Type-IV wind turbines. The approach does not require frequency-adaptive sampling to align the filter center frequency (unlike the DFT-based filters used in [13],[14]) nor pre-filters that lead to non-passive regions in the converter impedance that result from the cascaded filters used in [15]. The active filter permits narrow-band impedance shaping to increase harmonic damping and mitigate voltage amplification in WPPs. Furthermore, converter generated voltage harmonics are inherently eliminated within the narrow-band range, fitting naturally into the guideline that suppliers of energy should ensure good voltage quality [4]. Accordingly, WPPs (and other distributed generation (DG) sources) can benefit from incorporating the proposed active filter into their existing control. A simple tuning rule is developed by applying passivity-based analysis [16],[17] and more generally using the impedance-based stability criterion [18]. The performance of the active filter is verified through experiments on a 0.6MW Type-IV wind turbine.

II. Frequency Domain Modeling of WPPs

Consider Fig. 1a showing the three-phase grid-connected converter of a Type-IV wind turbine. All three-phase signals

are represented as complex signals i.e. $\mathbf{x}(t) = x_\alpha(t) + jx_\beta(t)$. The feedback signals are the line currents and phase voltages at the grid-side of the line inductor L, $\mathbf{i}(t)$ and $\mathbf{v}(t)$ respectively. $\mathbf{m}(t)$ is the modulating signal to the pulse-width modulation (PWM) unit.

A. Analysis of the Converter Impedance

Let the converter control be based on a stationary- or synchronous-frame current controller with voltage feed-forward as shown in Fig. 1b. $\mathbf{F}(s)$ and $\mathbf{G}(s)$ are complex transfer functions (given by the boldface) of the current controller and voltage feed-forward respectively. The active filter is introduced by the control signal $\mathbf{v}_{af}(s)$. The computational delay, digital PWM scheme and switching devices are modeled by the real transfer function $K(s)$ and the disturbance $\mathbf{v}_d(s)$ [19]. $K(s)$ is commonly modeled as a transport delay $\exp(-s1.5T_s) = \exp(-sT_d)$ where T_s is the sampling period of the converter [22]. This assumes that the modulating signal has been normalized by the DC-link voltage. $\mathbf{v}_d(s)$ represents the converter generated voltage harmonics i.e. sideband harmonics near multiples of the switching frequency and low-order harmonics due to non-ideal PWM pulse placement. The magnitude of the low-order voltage harmonics can vary depending on the modulation and sampling system, the dead-time placement scheme and any minimum switch on/off time constraints [19].

The frequency range of interest in this paper is $|f| \geq 150Hz$ hence effects of grid synchronization, which typically impact frequencies below $150Hz$, are ignored [8],[20],[21]. Similarly, the DC-link voltage and outer power/voltage controllers typically have low enough bandwidth that the reference current can be assumed to be null i.e. $\mathbf{i}_{ref}(s) = 0$ [17],[20].

Initially letting $\mathbf{v}_{af}(s) = 0$ and analyzing Fig. 1b in the Laplace domain gives

$$\mathbf{v}(s) + \underbrace{\left[\frac{sL + e^{-sT_d}\mathbf{F}(s)}{1 - e^{-sT_d}\mathbf{G}(s)}\right]}_{\mathbf{Z}(s)}\mathbf{i}(s) = \underbrace{\frac{\mathbf{v}_d(s)}{1 - e^{-sT_d}\mathbf{G}(s)}}_{\mathbf{e}(s)} \quad (1)$$

where $\mathbf{Z}(s)$ is the nominal converter impedance (the converter impedance without the active filter in service) and $\mathbf{e}(s)$ is the apparent harmonic voltage source generated by the converter. Fig. 1c shows the impedance model of the converter from (1) connected to a fictitious grid, where $Z_{txf}(s)$ is a transformer impedance, $Z_c(s)$ is a shunt impedance due to distributed capacitance and the AC grid is modeled as a Thevenin equivalent impedance $Z_g(s)$ and voltage source $\mathbf{v}_g(s)$.

B. Generation and Amplification of Harmonic Voltages

A pedagogical example of voltage amplification and its mitigation will be illustrated using the impedance model shown in Fig. 1c. The PCC voltage of interest is designated by $\mathbf{v}_{pcc}(s)$. The impact of converter and grid harmonic voltage sources on $\mathbf{v}_{pcc}(s)$ can be determined through voltage amplification factors. Let $A_1(s) = \mathbf{v}_{pcc}(s)/\mathbf{e}(s)$ and $A_2(s) = \mathbf{v}_{pcc}(s)/\mathbf{v}_g(s)$ be the voltage amplification factors due to converter and grid voltage sources respectively. Let $Z_{txf}(s) = Z_g(s)/2 = sL$ and $Z_c(s) = 1/(sC)$ with $L = 1\Omega$ and $C = 1$F. Fig. 2 shows the corresponding voltage amplification factors when $\mathbf{Z}(s) = 0$ and when $\mathbf{Z}(s) = 0.25\Omega$, highlighting the following points:

1) Voltage amplification can occur at different frequencies depending on the location of the harmonic source.
2) The amplifications tend to have a narrow-band peak.
3) A small increase in the damping provided by the converter can have a large impact on amplification factors.

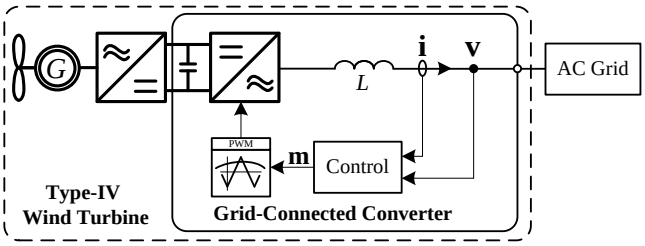

(a) Circuit diagram of the three-phase grid-connected converter of a Type-IV wind turbine.

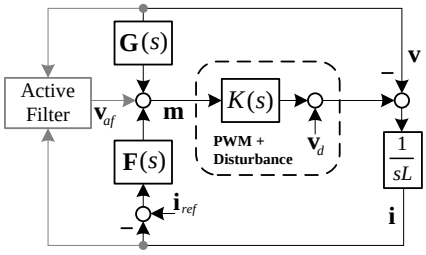

(b) Flow diagram of the converter control showing the main control being augmented by the active filter.

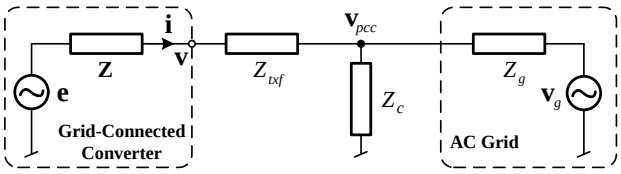

(c) Impedance model of the converter-grid system.

Fig. 1: Impedance modeling of a grid-connected converter used in a Type-IV wind turbine.

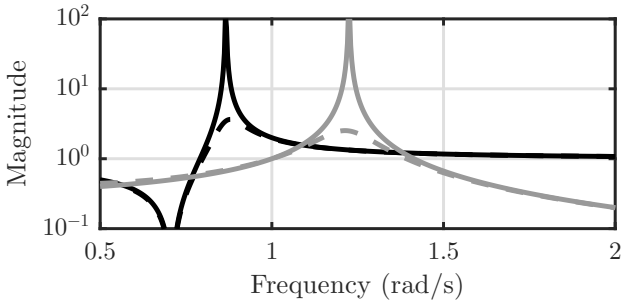

Fig. 2: Voltage amplification factors $|A_1(j\omega)|$ (——) and $|A_2(j\omega)|$ (——) when $\mathbf{Z}(s) = 0$, and $|A_1(j\omega)|$ (- - -) and similarly $|A_2(j\omega)|$ (- - -) when $\mathbf{Z}(s) = 0.25\Omega$.

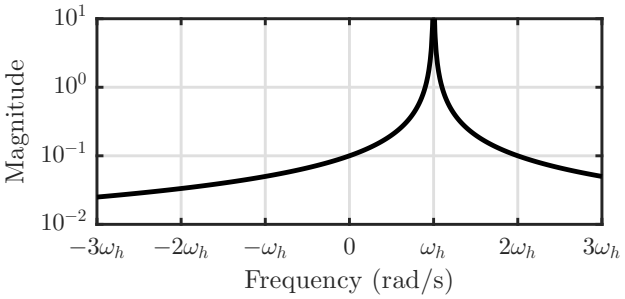

Fig. 3: Magnitude response of the complex resonator when $\omega_b = 0.1\omega_h$.

The aim now is to design an active filter that adds a prescribed amount of damping within a narrow frequency range, to mitigate large amplification factors at one or more points of common coupling. Furthermore, the active filter should help mitigate, as much as possible, the converter generated voltage harmonics. If this is achieved then damping is only needed for large amplification factors due to grid harmonics sources, simplifying the application of active filters in practice.

III. Design of a Complex Active Filter

A. Active Filter Control Law

The active filter control law is defined as

$$\mathbf{v}_{af}(s) = -\mathbf{C}_h(s)\left[\mathbf{v}(s) + Z_h\mathbf{i}(s)\right] \tag{2}$$

where Z_h is a programmed impedance (a complex number in the general case). $\mathbf{C}_h(s)$ is a complex resonator with center frequency ω_h and gain ω_b such that

$$\mathbf{C}_h(s) = e^{j\omega_h T_d}\frac{\omega_b}{s - j\omega_h} \tag{3}$$

where $\exp(j\omega_h T_d)$ provides the phase lead for compensation of computation and PWM delays. Delay compensation is vital in ensuring the stability of the converter, particularly when active filtering at high frequencies relative to the sampling frequency [16]. Note that if the voltage and current use different sampling methods, such as multiple sample and averaging [22], then different delay compensation may be required. Note that a complex resonator is used, as opposed to the ubiquities real-coefficient resonator, as infinite gain is only desired at the frequency for which Z_h is defined. The single resonant peak of the complex resonator is apparent in the magnitude response shown in Fig. 3 when $\omega_b = 0.1\omega_h$.

Updating (1) to include (2) gives

$$\mathbf{v}(s) + \underbrace{\left[\frac{sL + e^{-sT_d}\left(\mathbf{F}(s) + Z_h\mathbf{C}_h(s)\right)}{1 - e^{-sT_d}\left(\mathbf{G}(s) - \mathbf{C}_h(s)\right)}\right]}_{\mathbf{Z}_{af}(s)}\mathbf{i}(s) = \underbrace{\frac{\mathbf{v}_d(s)}{\left[1 - e^{-sT_d}\left(\mathbf{G}(s) - \mathbf{C}_h(s)\right)\right]}}_{\mathbf{e}_{af}(s)} \tag{4}$$

where $\mathbf{Z}_{af}(s)$ and $\mathbf{e}_{af}(s)$ are the converter impedance and apparent harmonic voltage source respectively with the active filter in service. When $s = j\omega_h$, (4) reduces to

$$\mathbf{v}(j\omega_h) + Z_h\mathbf{i}(j\omega_h) = 0 \tag{5}$$

highlighting two properties of the active filter:

1) The impedance is programmed to Z_h at $s = j\omega_h$.
2) The converter generated voltage harmonic is inherently eliminated at $s = j\omega_h$.

Therefore, the active filter can be used to ensure the voltage quality of a grid-connected converter even if impedance shaping is not required. This fits naturally with the concept that sources of energy (such as WPPs and DG units) should have as high voltage quality as possible [4].

Note that adding one or more active filters to the converter control increases changes the modulating signal. Therefore, a potential drawback of active filtering for a converter operating in the linear modulating range is that the maximum reactive power injection may be reduced.

B. Passivity of the Active Filter

Introducing an active filter changes the converter control structure and hence the passivity of the converter impedance [17], albeit within a narrow frequency range. The goal of a narrow-band active filter is to increase the real part of the nominal converter impedance $\mathrm{Re}\{\mathbf{Z}(j\omega)\}$ such that converter contributes additional damping to the power system at $\omega = \omega_h$. It is important, however, that the active filter does not degrade (or minimally degrades) passivity at neighboring frequencies [16]. To explore the influence of the active filter on passivity in a simplified manner let $T_d = 0$, $\mathbf{F}(s) = R$, $\mathbf{G}(s) = 0$ and $Z_h = R_h + jX_h$ such that

$$\mathbf{Z}_{af}(s) = (R + sL)\frac{s - j\omega_h}{s + \omega_b - j\omega_h} + Z_h\frac{\omega_b}{s + \omega_b - j\omega_h}. \tag{6}$$

When $s = j\omega$ the real part of (6) is

$$\begin{aligned}\mathrm{Re}\{\mathbf{Z}_{af}(j\omega)\} = K\Big[&(\omega - \omega_h)^2(R - \omega_b L) \\ &+ (\omega - \omega_h)\omega_b(X_h - \omega_h L) + R_h\omega_b^2\Big]\end{aligned} \tag{7}$$

where K is a positive constant. The converter impedance is passive at all frequencies, that is $\mathrm{Re}\{\mathbf{Z}(j\omega)\} \geq 0$, if the discriminant of (7) is less than zero i.e.

$$(X_h - \omega_h L)^2 - 4R_h(R - \omega_b L) < 0. \tag{8}$$

Equation (8) indicates that, for the simplified converter impedance, defining $X_h = \omega_h L$ is critical for maximizing converter passivity at frequencies neighboring $s = j\omega_h$. In general $X_h = \mathrm{Im}\{\mathbf{Z}(j\omega_h)\}$ should be used to take into account the existing converter control, giving the rule for passivity

$$Z_h = R_h + j\mathrm{Im}\{\mathbf{Z}(j\omega_h)\}. \tag{9}$$

C. Example of Impedance Shaping

Impedance shaping will now be applied to a 0.6MW current-controlled converter with the parameters given in Table I. The frequency response of the nominal converter impedance, shown in Fig. 4, is derived analytically from knowledge of the control transfer functions. An active filter is then added with center frequency $\omega_h = 7\omega_1$ and gain $\omega_b = 25$ rad/s.

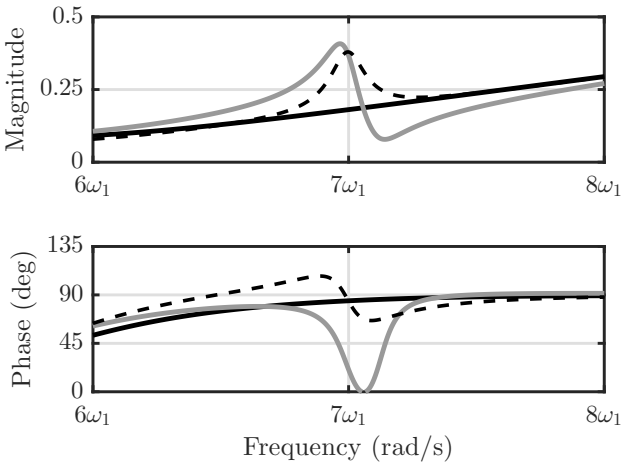

Fig. 4: Frequency response of the converter impedance with an active filter applied at $\omega = 7\omega_1$. Nominal impedance $\mathbf{Z}(j\omega)$ (——), $\mathbf{Z}_{af}(j\omega)$ with $Z_h = 2 \cdot \mathbf{Z}(j7\omega_1)$ (- - -) and $\mathbf{Z}_{af}(j\omega)$ with $Z_h = 0.3 + j\text{Im}\{\mathbf{Z}(j7\omega_1)\}$ (——).

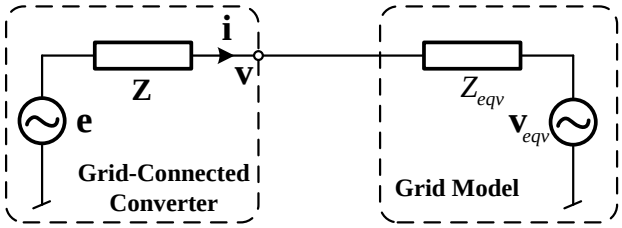

Fig. 5: Impedance model of a converter-grid system used for stability assessment.

First, $Z_h = 2 \cdot \mathbf{Z}(j7\omega_1)$ is programmed to double the overall magnitude of the converter impedance. As shown in Fig. 4, the programmed impedance is synthesized at $s = j\omega_h$ but the passivity of the converter is violated at neighboring frequencies (the phase exceeds $\pm 90°$). Next the passivity rule from (9) is applied by letting $Z_h = 0.3 + j\text{Im}\{\mathbf{Z}(j7\omega_1)\}$. In this case the damping has been increased at $s = j\omega_h$ but the converter impedance remains passive at neighboring frequencies.

Parameter	Value	Symbol
Rated active power	0.6 MW	P_{rated}
Rated frequency	$2\pi \cdot 50$ rad/s	ω_1
Rated voltage	690 V_{rms}	-
Line inductor	$5 - 15$ %	L

TABLE I: Parameters of the grid-connected converter.

D. Impedance-based Stability of the Active Filter

While (9) provides a straightforward rule for increasing converter damping at a given frequency it does not ensure stability of the converter-grid system. Therefore, a general method is required for determining the range of Z_h values that give a stable current response of the converter-grid system.

Consider Fig. 5 showing the converter impedance model connected to a Thevenin equivalent grid model given by $Z_{eqv}(s)$ and $\mathbf{v}_{eqv}(s)$. The converter current is determined as

$$\mathbf{i}(s) = \frac{\mathbf{e}(s) - \mathbf{v}_{eqv}(s)}{\mathbf{Z}(s)} \cdot \frac{1}{1 + Z_{eqv}(s)/\mathbf{Z}(s)}. \tag{10}$$

In the impedance-based stability criterion $Z_{eqv}(s)/\mathbf{Z}(s)$ must satisfy the Nyquist criterion for closed-loop stability of the converter-grid system [18]. Letting $\mathbf{Z}(s) = \mathbf{Z}_{af}(s)$ and splitting the impedance into two terms gives

$$\mathbf{Z}_{af}(s) = \underbrace{\frac{sL + e^{-sT_d}\mathbf{F}(s)}{1 - e^{-sT_d}\big(\mathbf{G}(s) - \mathbf{C}_h(s)\big)}}_{\mathbf{Z}_1(s)} + Z_h \underbrace{\frac{e^{-sT_d}\mathbf{C}_h(s)}{1 - e^{-sT_d}\big(\mathbf{G}(s) - \mathbf{C}_h(s)\big)}}_{\mathbf{Z}_2(s)}. \tag{11}$$

Equation (10) can then be rewritten as

$$\mathbf{i}(s) = \frac{\mathbf{e}(s) - \mathbf{v}_{eqv}(s)}{\mathbf{Z}_{af}(s)} \cdot \frac{1 + Z_h\mathbf{Z}_2(s)/\mathbf{Z}_1(s)}{1 + Z_{eqv}(s)/\mathbf{Z}_1(s)} \cdot \frac{1}{1 + Z_h\mathbf{D}(s)} \tag{12}$$

where

$$\mathbf{D}(s) = \frac{\mathbf{Z}_2(s)}{Z_{eqv}(s) + \mathbf{Z}_1(s)}. \tag{13}$$

Equation (12) features two feedback loops, both needing to satisfy the Nyquist criterion for stability of the converter-grid system. The first feedback loop $1/(1 + Z_{eqv}(s)/\mathbf{Z}_1(s))$ is primarily affected by the main converter control and assumed to be stable. In the second feedback loop $1/(1 + Z_h\mathbf{D}(s))$, Z_h scales the distance of $\mathbf{D}(j\omega)$ from the critical point -1. Therefore, a two-dimensional (complex) space of Z_h values that lead to $\mathbf{D}(j\omega)$ satisfying the Nyquist criterion can be defined as the points bounded by the complex function

$$\mathbf{S}(j\omega) = -\frac{1}{\mathbf{D}(j\omega)}. \tag{14}$$

The converter impedance defined in Section III-C is now used to illustrate the effect of Z_h on converter-grid stability. An active filter centered on the -5th harmonic and with $\omega_b = 25$ rad/s is added to the converter control. The equivalent impedance $Z_{eqv}(s)$ is comprised of the PWM filters used in the converter, an 0.8MVA transformer with 11% impedance and an RL grid with a short-circuit power of 46MVA and an X/R ratio of 7. The Nyquist diagram and stability boundary for Z_h are calculated from (13) and (14) respectively, and shown in Fig. 6. For a given real part, the stability boundary occurs when Z_h takes on a certain positive imaginary part (a capacitive impedance with respect to negative frequencies). This is because the grid appears predominantly inductive to the converter, hence programming the converter impedance to be capacitive can lead to a poorly damped LC resonance. The real part of Z_h (the damping term) can be increased from the nominal value without encroaching on the stability boundary.

The stability boundary predicted by $\mathbf{S}(j\omega)$ in Fig. 6 was tested in simulation. $Z_h = \mathbf{Z}(-j5\omega_1)$ was initially programmed, resulting in a stable time-domain response of $|\mathbf{i}(t)|$ as shown in Fig. 7. At $t = 0.3s$, $Z_h = j0.6$ was programmed

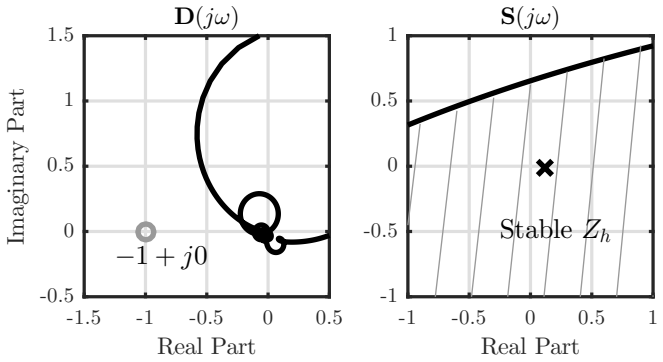

Fig. 6: Nyquist diagrams (left) and the stability boundary for Z_h (right) for an active filter centered on the -5th harmonic and with $\omega_b = 25$. The nominal converter impedance at the -5th harmonic is denoted by (✖).

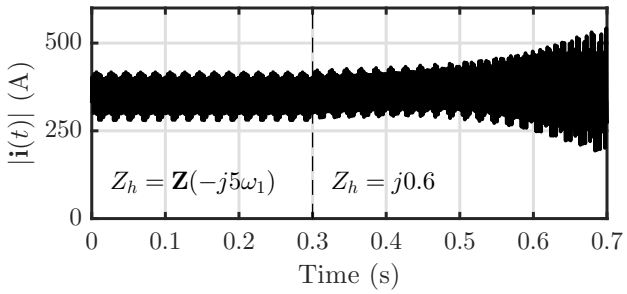

Fig. 7: Unstable response of the converter current when the active filter centered on the -5th harmonic is programmed at the stability limit with $Z_h = j0.6$.

which, according to Fig. 6, is on the stability boundary. The time-domain response in Fig. 7 exhibits growing oscillations as a result of the instability.

IV. Experimental Results

The active filter was tested on a 0.6MW grid-connected converter with parameters described in Table I and connected to the power grid in the UK. The complex voltages and currents, $\mathbf{v}(t)$ and $\mathbf{i}(t)$ respectively, were measured at the grid side of the main inductor L and post-processed by a fast Fourier transform (FFT). The FFT window was adapted to match the time-varying fundamental period of the measured signals. Therefore, the outputs of the FFT are the generalized voltage and current coefficients, $\mathbf{v}(h)$ and $\mathbf{i}(h)$ respectively, aligned at the harmonics of ω_1. The magnitude of the background voltage harmonics in the grid, shown in Fig. 8, were measured prior to connecting the converter.

A. Elimination of Converter Generated Voltage Harmonics

The sequence domain harmonic model [19] was used to calculate the apparent harmonic voltage source $\mathbf{e}(h)$ from the measured voltages and currents as

$$\mathbf{e}(h) = \mathbf{v}(h) + \mathbf{Z}(jh\omega_1)\mathbf{i}(h) \tag{15}$$

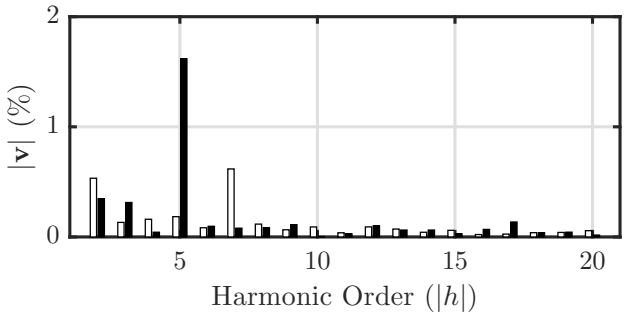

Fig. 8: Magnitude of the background harmonic voltages with the converter disconnected. $h < 0$ (▬) and $h > 0$ (▭).

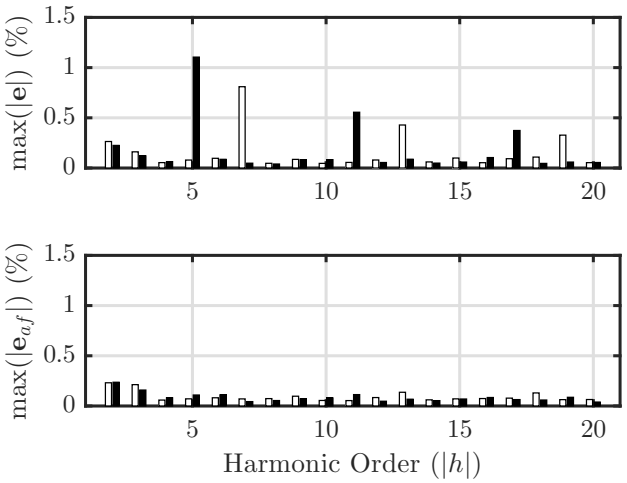

Fig. 9: Virtual spectrum of the worst-case apparent harmonic voltage sources taken across all measured power bins, without (top) and with (bottom) the active filter. $h < 0$ (▬) and $h > 0$ (▭).

where $\mathbf{Z}(jh\omega_1)$ is an offline calculation of the converter impedance at $s = jh\omega_1$. The apparent harmonic voltage source can then be compared with and without active filters in service. The results are presented through a virtual spectrum $\max(|\mathbf{e}(h)|)$ constructed of the harmonics with the largest magnitude found in $\mathbf{e}(h)$ over all tested operating points. The operating points are defined as 10% increments of rated active power injection. Therefore, eleven individual measurements were taken, ranging from $0\% \cdot P_{rated}, ..., 100\% \cdot P_{rated}$. The virtual spectrum with no active filters in service is shown in Fig. 9, highlighting the characteristic voltage harmonics generated by the converter.

Six instances of the voltage plus current active filter were then programmed, one targeting each of the characteristic odd harmonics of order $h = -17, -11, -5, 7, 13, 19$ and with $\omega_b = 25$ rad/s. The programmed impedance Z_h was set to the nominal converter impedance at that harmonic order i.e. $Z_h = \mathbf{Z}(jh\omega_1)$. As shown in Fig. 9, adding the active filters neutralized the targeted odd harmonics.

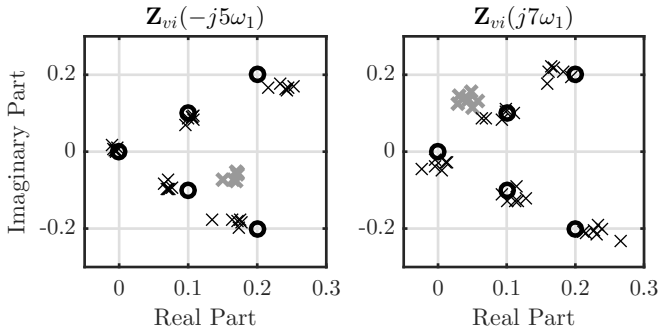

Fig. 10: Converter impedance shaping at the -5th and 7th harmonics. Estimated nominal impedance $\hat{\mathbf{Z}}(jh\omega_1)$ (✖), estimated impedance with active filter $\hat{\mathbf{Z}}_{af}(jh\omega_1)$ ($\times$) and the programmed impedance Z_h (O).

B. Impedance Shaping

As shown in Fig. 8, the -5th and 7th voltage harmonics in the external grid were of appreciable magnitude. Accordingly, these harmonic orders were targeted for testing the impedance shaping capability of the active filter. Two active filters targeting the -5th and 7th harmonics respectively were successively programmed to $Z_h = 0$, $Z_h = (0.1 \pm j0.1)\Omega$ and $Z_h = (0.2 \pm j0.2)\Omega$. The converter impedance was then estimated from the FFT data as $\hat{\mathbf{Z}}(jh\omega_1) = -\mathbf{v}(h)/\mathbf{i}(h)$. Fig. 10 shows the measured impedances against the programmed values. Note that the active filters correctly synthesized the programmed impedance regardless of the nominal converter impedance. This verifies that the converter can be used to synthesize a programmed amount of damping at a given frequency.

V. Conclusion

An impedance-based active filter based on a complex resonator was developed for the grid-connected converter in a Type-IV wind turbine. The active filter provided narrow-band impedance shaping and eliminated converter generated voltage harmonics. A passivity rule was proposed to increase the converter damping without compromising passivity at neighboring frequencies. The impedance-based stability criterion was also used to determine the programmed impedances that lead to a stable converter current response. The active filter was implemented on a 0.6MW grid-connected converter. The odd apparent harmonic voltage sources generated by the converter were compensated up to the 19th harmonic order. The converter impedance was also programmed at the -5th and 7th harmonic orders to specified values. The active filter can be used to improve the voltage quality of a grid-connected converter and/or increasing harmonic damping to mitigate voltage or current amplification that occur in WPPs.

Acknowledgment

This work was supported by Siemens Gamesa Renewable Energy A/S and the Innovation Fund, Denmark.

References

[1] J. Arrillaga and N. R. Watson, "Power System Harmonics," John Wiley & Sons Inc., Hoboken, NJ, USA, 2003.

[2] "Electromagnetic compatibility (EMC) - Part 3-6: Limits - Assessment of emission limits for the connection of distorting installations to MV, HV and EHV power systems," International Electrotechnical Commission Standard IEC-61000-3-6, 2008.

[3] "IEEE Recommended Practices and Requirements for Harmonic Control in Electrical Power Systems," IEEE Standard 519, 2014.

[4] H. Akagi, "Control strategy and site selection of a shunt active filter for damping of harmonic propagation in power distribution systems," IEEE Transactions on Power Delivery, vol. 12, no. 1, pp. 354–363, 1997.

[5] J. H. R. Enslin and P. J. M. Heskes, "Harmonic interaction between a large number of distributed power inverters and the distribution network," vol. 4, pp. 1742–1747, 2003.

[6] S. Zhang, S. Jiang, X. Lu, B. Ge, and F. Z. Peng, "Resonance issues and damping techniques for grid-connected inverters with long transmission cable," IEEE Transactions on Power Electronics, vol. 29, no. 1, pp. 110–120, Jan. 2014.

[7] Z. Shuai, D. Liu, J. Shen, C. Tu, Y. Cheng, and A. Luo, "Series and parallel resonance problem of wideband frequency harmonic and its elimination strategy," IEEE Transactions on Power Electronics, vol. 29, no. 4, pp. 1941–1952, Apr. 2014.

[8] E. Ebrahimzadeh, et. al., "Harmonic stability and resonance analysis in large PMSG-based wind power plants," IEEE Transactions on Sustainable Energy, vol. 9, no. 1, pp. 12–23, Jan. 2018.

[9] L. H. Kocewiak, et. al., "Power quality improvement of wind power plants by active filters embedded in STATCOMs," in Proc. The 15th International Workshop on Large-Scale Integration of Wind Power into Power Systems, Vienna, Austria, Nov. 2016.

[10] S. K. Chaudhary, C. Lascu, R. Teodorescu, and L. Kocewiak, "Voltage feedback based harmonic compensation for an offshore wind power plant," IEEE International Conference on Power Electronics, Drives and Energy Systems (PEDES), pp. 1–5, Dec. 2016.

[11] L. H. Kocewiak, et. al., "Active filtering application in large offshore wind farms," in Proc. The 13th International Workshop on Large-Scale Integration of Wind Power into Power Systems, 11-13 November 2014, Berlin, Germany.

[12] X. Wang, Y. Li, F. Blaabjerg, and P. C. Loh, "Virtual-impedance-based control for voltage-source and current-source converters," IEEE Transactions on Power Electronics, pp. 1–1, 2014.

[13] J. He, Y. W. Li, and M. S. Munir, "A flexible harmonic control approach through voltage-controlled DG-grid interfacing converters," IEEE Transactions on Industrial Electronics, vol. 59, no. 1, pp. 444–455, Jan. 2012.

[14] M. Cespedes and Jian Sun, "Mitigation of inverter-grid harmonic resonance by narrow-band damping," IEEE Journal of Emerging and Selected Topics in Power Electronics, vol. 2, no. 4, pp. 1024–1031, Dec. 2014.

[15] X. Wang, F. Blaabjerg, and Z. Chen, "Synthesis of variable harmonic impedance in inverter-interfaced distributed generation unit for harmonic damping throughout a distribution network," IEEE Transactions on Industry Applications, vol. 48, no. 4, pp. 1407–1417, Jul. 2012.

[16] L. Harnefors, et. al., "Passivity-based controller design of grid-connected VSCs for prevention of electrical resonance instability," IEEE Transactions on Industrial Electronics, vol. 62, no. 2, pp. 702–710, Feb. 2015.

[17] L. Harnefors, X. Wang, A. G. Yepes, and F. Blaabjerg, "Passivity-based stability assessment of grid-connected VSCs—an overview," IEEE Journal of Emerging and Selected Topics in Power Electronics, vol. 4, no. 1, pp. 116–125, Mar. 2016.

[18] J. Sun, "Impedance-based stability criterion for grid-connected inverters," IEEE Transactions on Power Electronics, vol. 26, no. 11, pp. 3075–3078, Nov. 2011.

[19] E. Guest, K. H. Jensen, and T. W. Rasmussen, "Sequence domain harmonic modeling of Type-IV wind turbines," IEEE Transactions on Power Electronics, vol. 33, no. 6, June 2018.

[20] M. Cespedes and J. Sun, "Impedance modeling and analysis of grid-connected voltage-source converters," IEEE Transactions on Power Electronics, vol. 29, no. 3, pp. 1254–1261, Mar. 2014.

[21] M. K. Bakhshizadeh et al., "Couplings in phase domain impedance modelling of grid-connected converters," IEEE Transactions on Power Electronics, pp. 1–1, 2016.

[22] S. Buso and P. Mattavelli, "Digital Control in Power Electronics, 2nd Edition," Morgan & Claypool, USA, 2015.